Supporting Information

# Effect of inorganic salt blending on the $CO_2$ separation performance and morphology of Pebax®1657/ ionic liquid gel membranes

Winny Fam[a], Jaleh Mansouri[a*], Hongyu Li[a], Jingwei Hou[b] and Vicki Chen[a,c]

[a] UNESCO Centre for Membrane Science and Technology, School of Chemical engineering, University of New South Wales, Sydney, New South Wales 2052, Australia

[b] Department of Materials Science and Metallurgy, University of Cambridge, Cambridge CB3 0FS, U.K.

[c] School of Chemical Engineering, University of Queensland, St. Lucia, Queensland 4072, Australia

[*] Corresponding author: j.mansouri@unsw.edu.au

1. Composition of Pebax/IL/inorganic salt solutions for membrane casting and selective layer coating.

**Table S1**. Composition of Pebax/IL/inorganic salt solutions in 87.6 g ethanol/water (70:30)

| Solution | Pebax (g) | IL (g) | Inorganic salt (mg) |
|---|---|---|---|
| Pebax/NaCl (70:1) | 2.61 | 0 | 29.7 |
| Pebax/$Na_2SO_4$ (70:1) | 2.61 | 0 | 72.1 |
| Pebax/$CaCl_2$ (70:1) | 2.61 | 0 | 56.4 |
| Pebax/$CaCl_2$ (45:1) | 2.61 | 0 | 87.7 |
| Pebax/$CaCl_2$ (30:1) | 2.61 | 0 | 132 |
| Pebax/$CaCl_2$ (15:1) | 2.61 | 0 | 263 |
| Pebax/IL40/$CaCl_2$ (30:1) | 2.61 | 1.83 | 132 |
| Pebax/IL80/$CaCl_2$ (30:1) | 2.61 | 11.0 | 132 |

2. Schematic diagram of free-standing membrane casting and hollow fiber dip coating.

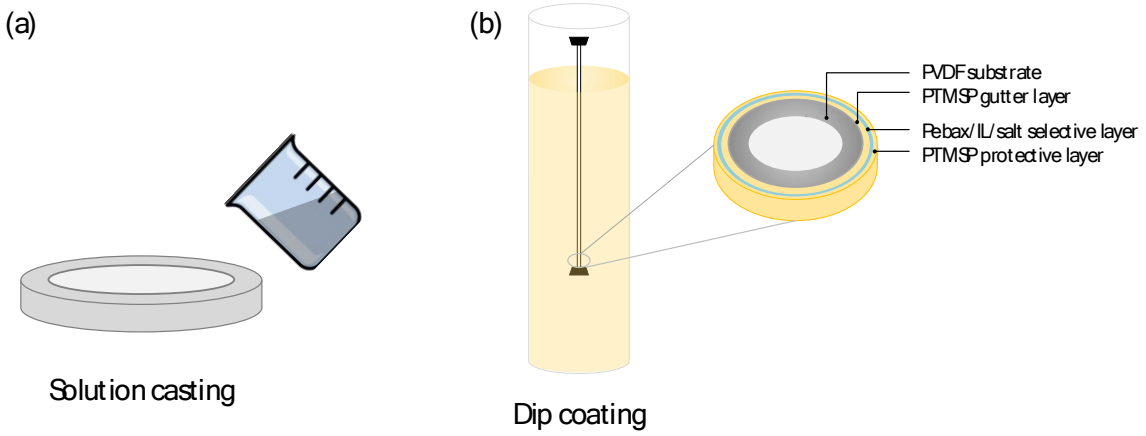


**Figure S1.** Schematic diagram of membrane fabrication: (a) fabrication of free-standing membrane using solution casting and (b) fabrication of thin film composite membrane using dip coating.

3. Schematic diagram of constant-pressure-variable-volume gas permeation test with humidified feed.

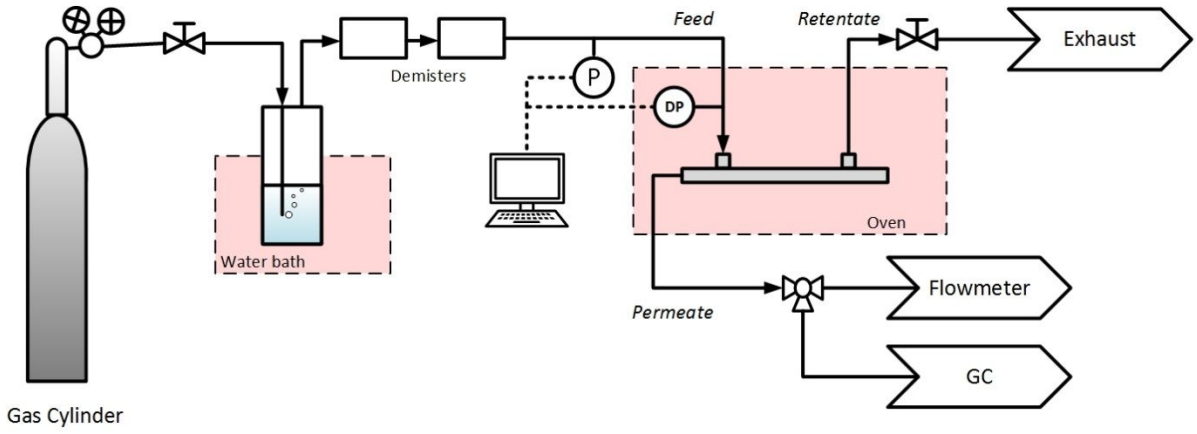


**Figure S2.** Schematic diagram of gas permeation test.

## 4. Dense membrane characterization

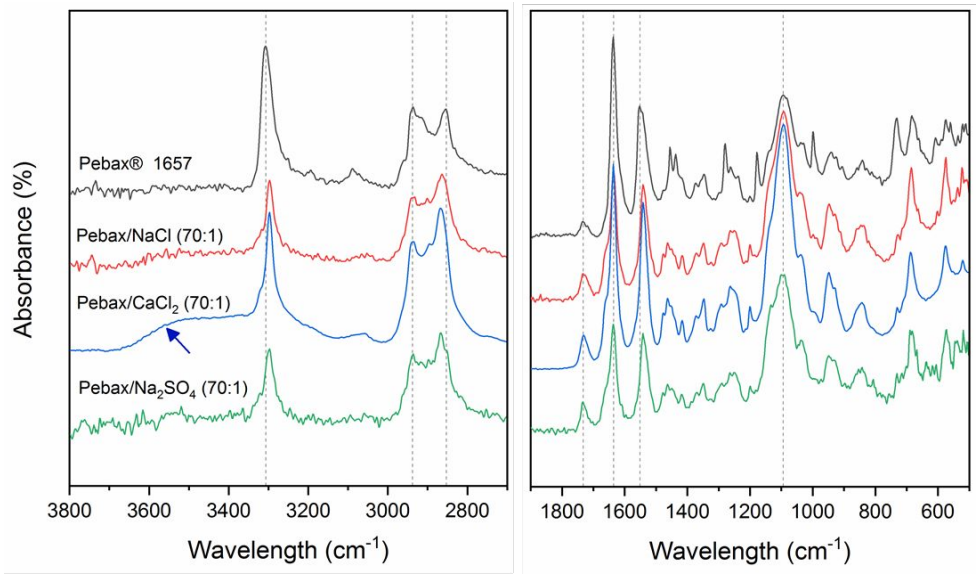


**Figure S3.** FTIR spectra of dense neat Pebax and Pebax/inorganic salt membranes (70:1)

Figure S3 shows the main peaks on Pebax spectra at 3307, 1733, 1636, 1552, and 1094 $cm^{-1}$, which were assigned to N-H stretching, free C=O stretching, N-H bending, N-H···C=O (amide II) and C-O stretching vibrations, respectively.[1] The emergence and weakening of peaks on Pebax/ inorganic salt spectra in the range from 1500-1200 $cm^{-1}$ and 900-500 $cm^{-1}$ can be assigned to the interaction between the ions and Pebax segments.[2] The broad peak at 3500 $cm^{-1}$ on $CaCl_2$-doped membrane, which is marked by the arrow on the spectra, was assigned to O-H stretching.

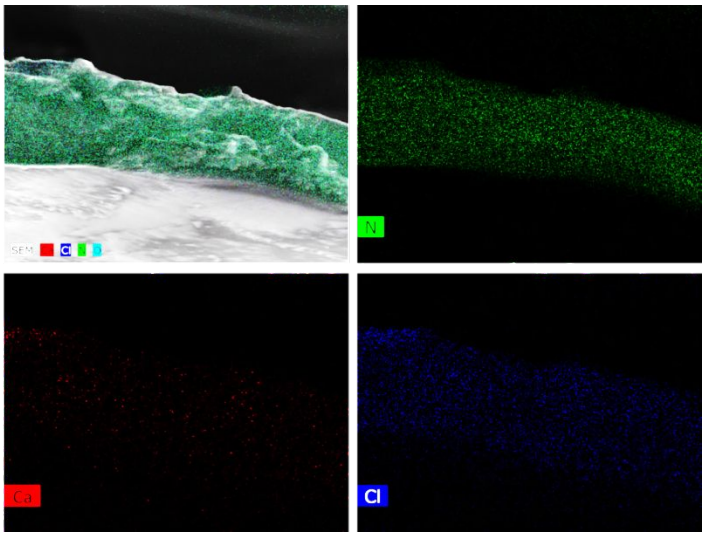


**Figure S4**. EDS cross section scan of dense Pebax/$CaCl_2$ (15:1) membrane.

Figure S4 shows the elemental scan of Pebax/$CaCl_2$ (15:1) membrane. The nitrogen signal represents the PA6 segment of Pebax, whereas Ca and Cl signals represent the inorganic salt. Uniform elemental distributions can be observed throughout the membrane thickness.

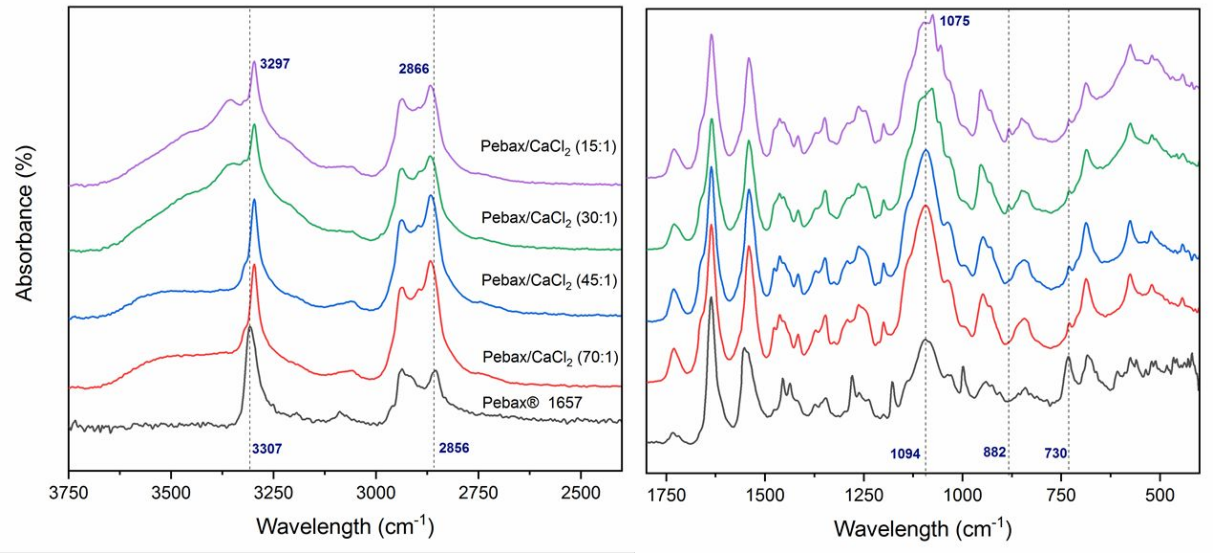


**Figure S5.** FTIR spectra of neat Pebax and Pebax/$CaCl_2$ membranes

The interactions between the block copolymer segments and the $CaCl_2$ salt ions with increasing salt concentration were investigated using FTIR, as shown in Figure S5. The symmetrical bending vibration of –$(CH_2)$– at 2857 $cm^{-1}$ found in both Pebax segments shifted to the higher wavelength at 2866 $cm^{-1}$ in $CaCl_2$-doped membranes. In addition, the peak at 730 $cm^{-1}$ assigned to the plane vibration of –$(CH_2)_5$– weakened[3] and the N-H stretch peak at 3307 $cm^{-1}$ shifted to 3297 $cm^{-1}$ in all of $CaCl_2$-doped membranes, which suggests a complexation between $Ca^{2+}$ and PA6 segment. The wide C-O stretching vibration of the PEO segment at 1094 $cm^{-1}$ for neat Pebax shifted to 1075 $cm^{-1}$ for Pebax/$CaCl_2$ (30:1) and (15:1). The shift may be due to the complexation between the PEO segments and the cations, which disrupts the existing interchain hydrogen bonding in Pebax.

5. TFC membrane characterization

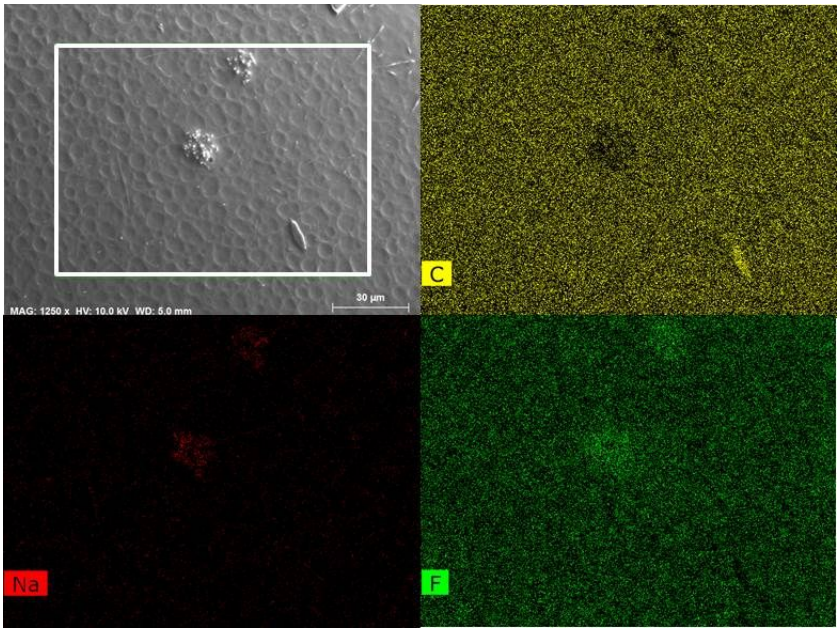


**Figure S6**. EDS elemental scan of Pebax/IL80/$Na_2SO_4$ (70:1) TFC membrane.

Figure S6 shows the elemental distribution on the surface of Pebax/IL80/$Na_2SO_4$ (70:1). Some area showed that the signal from Na corresponded to a stronger signal of F, which represented $BF_4$, suggesting the formation of $NaBF_4$. Table S2 shows the roughness and surface area of each TFC membrane based on the projected area of $1\mu m^2$.

**Table S2**. Roughness and surface area of TFC Pebax/IL/inorganic salt membranes with PEO: inorganic salt loading of 30:1.

| TFC Selective layer | Ra (nm) | Rms (nm) | Surface area ($\mu m^2$) |
|---|---|---|---|
| Pebax/NaCl | 11.0±0.9 | 14.4±0.5 | 1.09±0.02 |
| Pebax/IL40/NaCl | 20.1±1.1 | 26.8±1.3 | 1.18±0.08 |
| Pebax/IL80/NaCl | 30.9±1.2 | 38.1±1.4 | 1.59±0.22 |
| Pebax/$CaCl_2$ | 12.6±0.2 | 15.6±0.2 | 1.06±0.15 |
| Pebax/IL40/CaCl2 | 14.0±0.1 | 16.1±0.1 | 1.03±0.01 |
| Pebax/IL80/$CaCl_2$ | 17.4±1.3 | 21.1±1.2 | 1.21±0.04 |
| Pebax/$Na_2SO_4$ | 9.0±0.5 | 12.3±0.7 | 1.11±0.06 |
| Pebax/IL40/$Na_2SO_4$ | 13.9±0.6 | 18.0±0.7 | 1.09±0.01 |
| Pebax/IL80/$Na_2SO_4$ | 10.4±0.9 | 15.8±0.1 | 1.12±0.08 |

## 6. Contribution of PTMSP aging to the overall performance

For the TFC membranes fabricated for this work, a significant decrease in gas permeation performance associated with the aging of the PTMSP gutter layer has been consistently observed. In fact, the notorious aging characteristic of PTMSP has been reported in many studies.[4–6] The aging rate is known to be highly dependent on the membrane thickness. For instance, Chen et al. reported 80% decrease in $CO_2$ permeance through 1-$\mu$m PTMSP layer on PAN hollow fiber after only 14 days,[6] whereas Sutrisna et al. observed that the decrease experienced by 7-$\mu$m PTMSP layer coated on PVDF hollow fibers was only 22% for the same permeation test duration.[7] In the same study, however, Sutrisna et al. reported a stable performance of the Pebax TFC membranes using PTMSP gutter layer and hypothesized that the stable performance was due to the Pebax penetration and polymer entanglements at the interface, similar to the confinement effect via the formation of multi-layered glassy/rubbery polymer films observed by Murphy et al.[8] Furthermore, PTMSP contact with ethanol during the formation of Pebax selective layer may also contribute to reversing the physical aging to some extent.[9,10]

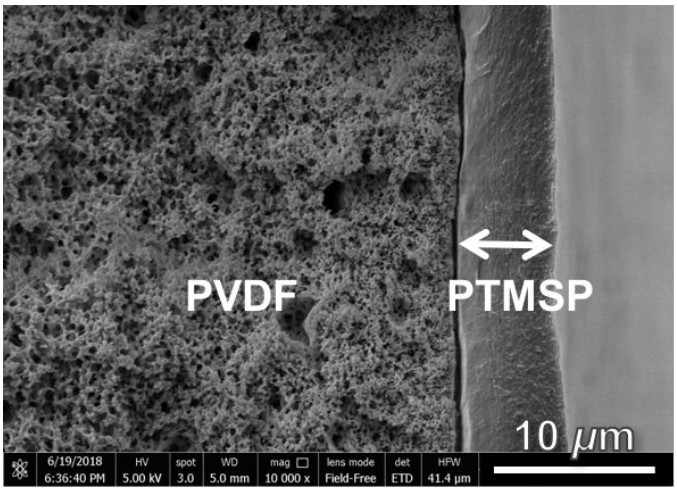


**Figure S7**. SEM cross-sectional image of the PTMSP-coated hollow fiber for the aging study. The thickness of the PTMSP layer is approximately 6.1 $\mu$m.

To quantify and investigate the contribution in the decrease in gas permeance due to PTMSP aging, the $CO_2$ separation performance of PTMSP TFC hollow fibers were monitored periodically for over 400 days. The thickness of the PTMSP layer based on the cross-sectional SEM image is approximately 6.1 $\mu$m (Fig. S7). The performance of the PTMSP composite hollow fibers is given in Figure S7a. The initial $CO_2$ permeance of the fibers at 2715 GPU was recorded on day 12 after the fabrication, which is equivalent to 16,443 barrer. This value is significantly lower than the reported $CO_2$ permeability value of thick PTMSP film at 28,000 barrer[11] (or 4623 GPU for 6.1-$\mu$m thick film). This suggests a permeance loss of approximately 40% in the first 12 days although the aging occurs at a slower rate in the following 400 days, leading to a total of 52% decrease. It is therefore important to take the aging behavior of the gutter layer into account when evaluating and reporting the performance of the TFC membranes.

The contribution of the PTMSP layer to the total resistance $R_T$ of the TFC membrane is calculated based on the sum of resistance in series, as follows:

$$R_T = R_g + R_s + R_p = \frac{1}{A}\left[\left(\frac{\ell}{P}\right)_g + \left(\frac{\ell}{P}\right)_s + \left(\frac{\ell}{P}\right)_p\right] \quad (1)$$

$$\frac{1}{J} = \left[\left(\frac{\ell}{P}\right)_g + \left(\frac{\ell}{P}\right)_s + \left(\frac{\ell}{P}\right)_p\right] \quad (2)$$

where $J$ is the measured gas flux, $\ell/P$ is the inverse of the gas permeance, and the subscripts $g$, $s$ and $p$ refer to gutter, selective and protective layer, respectively. It is assumed that the cross sectional area $A$ remains constant for each layer and the contribution of the porous substrate is negligible. Additionally, the total thickness of the PTMSP protective and gutter layers is assumed to be 5 $\mu$m, and the aging behavior follows the trend presented in Figure S8a. Using the measured flux of Pebax/IL80/$CaCl_2$ (30:1) of 899 GPU and theoretical flux of PTMSP gutter and protective layers of 5600 GPU, the resistance of the selective layer was calculated and presented in Figure S8b.

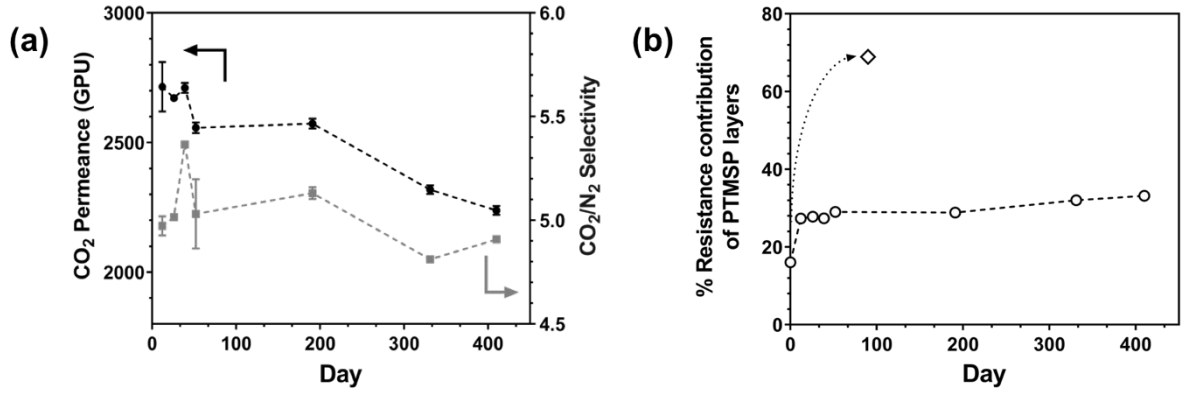


**Figure S8**. (a) Long-term performance of PTMSP coated on PVDF hollow fiber with feed gas pressure of 1 bar at room temperature. (b) Calculated resistance contribution of PTMSP layers (gutter + protective) to the $CO_2$ permeance through Pebax/IL80/$CaCl_2$ (30:1) TFC membranes using the reported intrinsic permeability of PTMSP. The diamond symbol represents the resistance contribution based on the actual performance of the same TFC membranes after 3 months.

The PTMSP layer resistance initially made up 16% of the total resistance, and it contributed to 33% of the total resistance after 1 year. However, the diamond symbol in the figure, which was calculated based on the real performance of the fibers after 3 months (369 GPU), represents 70% resistance contribution of the PTMSP layers. This confirms that the actual aging of the PTMSP layers in the Pebax/IL/inorganic salt TFC hollow fibers was more severe. Some factors that may promote the accelerated aging behavior of the overall TFC membranes include the rapid aging of the thin protective layer, the aging of the selective layer or loss of IL, and the aging behavior of PTMSP in contact with IL, which has not been investigated. Although studying the effect of each factor is beyond the scope of this work, it should be considered in future studies to obtain a better understanding and develop better strategies for ultrapermeable TFC membrane fabrication.

## References

(1) Qiu, Y.; Ren, J.; Zhao, D.; Li, H.; Deng, M. Poly(Amide-6-b-Ethylene Oxide)/[Bmim][$Tf_2N$] Blend Membranes for Carbon Dioxide Separation. *J. Energy Chem.* **2016**, *25* (1), 122–130.

(2) Li, Y.; Xin, Q.; Wu, H.; Guo, R.; Tian, Z.; Liu, Y.; Wang, S.; He, G.; Pan, F.; Jiang, Z. Efficient $CO_2$ Capture by Humidified Polymer Electrolyte Membranes with Tunable Water State. *Energy Environ. Sci.* **2014**, *7* (4), 1489.

(3) Li, X.H.; Deng, S.D.; Fu, H.; Mu, G.N. Inhibition by Tween-85 of the Corrosion of Cold Rolled

Steel in 1.0 M Hydrochloric Acid Solution. *J. Appl. Electrochem.* **2009**, *39* (7), 1125–1135.

(4) Dorkenoo, K. D.; Pfromm, P. H. Accelerated Physical Aging of Thin Poly[1-(Trimethylsilyl)-1-Propyne] Films. *Macromolecules* **2000**, *33* (10), 3747–3751.

(5) Lau, C. H.; Nguyen, P. T.; Hill, M. R.; Thornton, A. W.; Konstas, K.; Doherty, C. M.; Mulder, R. J.; Bourgeois, L.; Liu, A. C. Y.; Sprouster, D. J.; et al. Ending Aging in Super Glassy Polymer Membranes. *Angew. Chemie - Int. Ed.* **2014**, *53* (21), 5322–5326.

(6) Chen, H. Z.; Thong, Z.; Li, P.; Chung, T.-S. High Performance Composite Hollow Fiber Membranes for CO2/H2 and CO2/N2 Separation. *Int. J. Hydrogen Energy* **2014**, *39* (10), 5043–5053.

(7) Sutrisna, P. D.; Hou, J.; Li, H.; Zhang, Y.; Chen, V. Improved Operational Stability of Pebax-Based Gas Separation Membranes with ZIF-8: A Comparative Study of Flat Sheet and Composite Hollow Fibre Membranes. *J. Memb. Sci.* **2017**, *524*, 266–279.

(8) Murphy, T. M.; Langhe, D. S.; Ponting, M.; Baer, E.; Freeman, B. D.; Paul, D. R. Physical Aging of Layered Glassy Polymer Films via Gas Permeability Tracking. *Polymer (Guildf).* **2011**, *52* (26), 6117–6125.

(9) Merkel, T. C.; Bondar, V.; Nagai, K.; Freeman, B. D. Sorption and Transport of Hydrocarbon and Perfluorocarbon Gases in Poly(1-Trimethylsilyl-1-Propyne). *J. Polym. Sci. Part B Polym. Phys.* **2000**, *38* (2), 273–296.

(10) Bazhenov, S. D.; Borisov, I. L.; Bakhtin, D. S.; Rybakova, A. N.; Khotimskiy, V. S.; Molchanov, S. P.; Volkov, V. V. High-Permeance Crosslinked PTMSP Thin-Film Composite Membranes as Supports for CO2 Selective Layer Formation. *Green Energy Environ.* **2016**, *1* (3), 235–245.

(11) Stern, A. Polymers for Gas Separations: The next Decade. *J. Memb. Sci.* **1994**, *94* (1), 1–65.